Surface Characteristics and Rose Bengal Adsorption Studies of Carbon Nanospheres Synthesized via Atmospheric Combustion of Diesel

Article *in* IOP Conference Series Materials Science and Engineering · November 2020

DOI: 10.1088/1757-899X/928/5/052029

CITATIONS
0

READS
28

5 authors, including:

Ibrahim Sahib
University of Alkafeel
4 PUBLICATIONS **8** CITATIONS

SEE PROFILE

Hassan Alshamsi
University of Al-Qadisiyah
60 PUBLICATIONS **75** CITATIONS

SEE PROFILE

Surface Characteristics and Rose Bengal Adsorption Studies of Carbon Nanospheres Synthesized via Atmospheric Combustion of Diesel

IOP Conf. Series: Materials Science and Engineering **928** (2020) 052029 doi:10.1088/1757-899X/928/5/052029

Surface Characteristics and Rose Bengal Adsorption Studies of Carbon Nanospheres Synthesized via Atmospheric Combustion of Diesel

Salam Hussein Alwan[1], Muhammed Abbas Al Bedairy[2], Ibrahim Jooda Sahib[3], Hassan Abbas Alshamsi*[4]

[1]College of Dentistry, University of Al-Qadisiyah, Diwaniya, Iraq

[2]Ministry of Education - General Directorate of AL- Qadisiyah Education, Diwaniya, Iraq

[3]College of Dentistry, Alkafeel University, Najaf, Iraq

[4]Department of Chemistry, College of Education, University of Al-Qadisiyah, Diwaniya, Iraq

[5]College of Biotechnology, University of Al-Qadisiyah, Diwaniya, Iraq

[*]**Corresponding author**:

E-mail addresses: hasanchem70@gmail.com

Abstract

In this study, the carbon nanospheres were synthesized by burning diesel and then treated with hydrogen peroxide (H_2O_2). The results showed that H_2O_2 - carbon nanospheres has a higher surface area than carbon nanospheres and therefore it was chosen as an adsorbent surface to remove the Rose Bengal dye from aqueous solutions. The prepared carbon nanospheres were examined by FTIR, XRD, SEM, AFM, TGA, Raman spectroscopy, BET and EDX. The FTIR study reveals the presence of hydroxyl and carboxyl stretching vibration and weak peaks belong to CH_3, CH_2 and C=C. Results obtained by Raman and XRD analysis are in good agreement thereby indicating the amorphous structure of the carbon nanospheres. Also, SEM images confirm the presence of soot materials as spherical and semispherical nanoparticles with diameter in the range (31-78 nm). Surface roughness calculated from AFM data provided evidence that spiky appearance on both carbon surfaces. TGA data indicate that both carbon samples are thermally unstable. BET and BJH results indicate that the treated sample possesses the highest surface area and mean pore diameter. EDX analysis indicated the presence of pure carbon nanosphere (treated sample) without any contamination. Also, the adsorptive removal of Rose Bengal on synthesized carbon nanospheres was studied. The isotherm adsorption results were found to be described fitted by the Freundlich rather than the Langmuir and Temkin models. Furthermore, the kinetics of dye adsorption were applied better by the pseudo-second-order model.

Key words: Diesel oil, Combustion, Carbon nanospheres, Adsorption, Rose Bengal

1. Introduction

Carbon nanoparticles (CNPs) have attained an extensive research interest of researchers in recent years due to their excellent photoluminescent, good electrical/thermal conductivity, high porosity/surface area, good chemical/bio compatibility and high chemical/photo stability (1-3). The exceptional physical and chemical properties of carbon materials, make these materials appropriate for use in a variety of application fields like polymer composites (4), catalysis (5), filtration (6), adsorption(7), clean energy (8) and drug-loading (9). Appropriate use of carbon nanoparticles is fundamentally depends on their properties and relatively on simplicity, efficiency, scalability and affordability of synthesis techniques (10). Carbon nanoparticles can be synthesized using different methods with desired particle size, shape and composition depend on the control of factors such as temperature and type of organic species (11). Materials such as paraffin wax (2), ethanol (12), methane (13), benzene (14), kerosene (15), diesel oil (16), lubricant oil (17) and acetylene (18) are a major cheap and available sources for synthesis of spherical and small size carbon nanoparticles via incomplete combustion/pyrolysis processes. Carbon nanoparticles can grow on the ceramic plates, fire bricks, metals and any other produced materials in the combustion area. Most carbon nanoparticles synthesized from hydrocarbons characterized by high surface hydrophobicity which due to their low content of hydroxyl and carboxyl groups (19). Beside incomplete combustion process CNPs can be fabricated by a variety of techniques and procedures such as arc-discharge(20), laser ablation (21), chemical vapor deposition (CVD)(22), hydrothermal (23), microwave (24) and ultrasonic (25).

The present work aims to synthesis of carbon nanospheres by the incomplete combustion of Iraqi diesel oil and their structural, thermal, topological and morphological properties were investigated by means of FTIR, XRD, SEM, AFM, TGA, Raman spectroscopy, BET and EDX. Also, the exploring of adsorption of Rose Bengal dye (RB) from aqueous solution by synthesizing carbon materials was studied. The removal of RB on treated carbon sample was investigated as a function of parameters such as contact time, adsorbent loading, temperature, acidic function and ionic strength. To investigate the mechanism and adsorptive nature of the treated carbon nanospheres, different isotherms and kinetic models were applied, whereas thermodynamic study was used to predict the adsorption spontaneity.

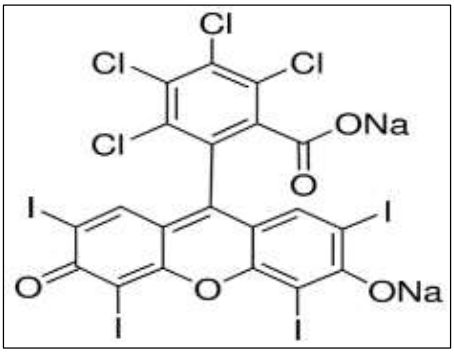

Fig. 1. Rose Bengal dye structure

2. Experimental

2.1. Chemicals: Diesel oil produced by the South Refineries Company, Iraq. Other chemical used are ethanol (Scharlau 99.9%), acetone (Scharlau 99%) and hydrogen

peroxide (Sigma Aldrich 35%) were used without further purification. Rose Bengal dye, so known as Acid Red 949, IUPAC Name: 4,5,6,7–Tetra chloro – 3',6'–dihydroxy-2',4',5',7'-tetraiodo – 3H- Spiro [isobenzofuran-1,9'- xanthen]-3-one] (empirical formula: $C_{20}H_2Cl_4I_4Na_2O_5$, molecular weight: 1017.64 g/L, dye content: 95 %) was purchased from Merck. All solutions were prepared using double distilled water (DDW).

2.2. Characterization of Carbon Nanoparticles

Fourier transform infrared spectroscopy (FTIR) analysis was performed by a Shimadzu FTIR 8000 Series with KBr disks as sample holders in the range 4000-400 cm^{-1}. Crystallinity of the samples has been characterized by X-ray diffraction (XRD) analysis using a D/Max 2.550 V diffractometer with Cu Kα radiation (λ = 1.54056 Å) (Rigaku, Tokyo, Japan) and the 60 XRD data were collected at a scanning rate of 0.03 s^{-1} for 2θ in a range from 5° to 80°. The shapes of as synthesized materials were analyzed by scanning electron microscopy (TESCAN VEGA3). Atomic force microscopy (AFM) was conducted using a Park Systems XE-70 Atomic Force Microscope in non-contact style. Thermo gravimetric analysis was employed on LINSEIS-STA PT-1000 with 5-20 mg samples and a heating rate of 10 $^oC\ min^{-1}$ from 50 to 600 ^oC in an Ar atmosphere. The Raman spectra were recorded by Jobin-Yvon HR800 UV-VIS-NIR Raman spectrometer. Nitrogen adsorption/ desorption isotherms were used to study the Brunauer- Emmett- Teller (BET) surface area and pore size. Rose Bengal absorbance was recorded using a Shimadzu UV-Vis 160V spectrophotometer.

2.3. Synthesis of Carbon Nanospheres

The carbonization of diesel was carried out according to previous report with some modification (26). Simple lamp equipped with combustible cylindrical, cotton material (wick) and Pyrex beaker were finely cleaned with detergent followed by acetone and were dried in oven at 120 °C. Commercial diesel oil was put in lamp with a wick and it was left for 24 h to saturation of wick with diesel oil .The wick was fired and a Pyrex beaker was placed over the flame to collect carbon emitted from the lamp and to prevent the excess air oxygen. When an amount of carbon approximately equal to 10 g was collected, the burning process was terminated. The black material was collected, washed with ethanol and acetone several times, then it was separated by centrifuge at 8000 rpm. 3 g of carbonaceous material was mixed with 50 mL of 10% hydrogen peroxide (H_2O_2) and sonicated for 2h (Labtec-410 sonication bath), it was then separated by centrifuge at 8000 rpm. The soot named as **PC**: pristine carbon nanospheres and **HC**: carbon nanospheres treated with H_2O_2.

2.4. Adsorption Study

Stock solution of 1000 mg/L was prepared by dissolving 1 g of RB dye in 1000 mL of double distilled water. Required experimental concentrations were prepared by dilution of stock solutions in as appropriate volume of DDW.

Dye solutions (10 mL) of known concentrations 5-200 ppm were transferred into stoppered conical flasks containing 0.01 g of carbon nanospheres (**HC)**. The conical flasks are stirred using Thermostatic Digital Laboratory Water Bath until they

reach equilibrium at a speed of 150 rpm. Therefore, the equilibrium time is the appropriate time to saturate the surface adsorbed with the adsorbed particles in the adsorption process. After equilibrium, solutions are separated at speeds of 6000 rpm in the centrifuge for 10 minutes. The equilibrium concentration of the solution was determined by using UV-Visible spectroscopy at dye λ_{max} (546 nm), after separation of the supernatant. Equilibrium concentrations were obtained by comparing the experimental data with the calibration curve. The quantity of dye adsorbed was calculated according to the following equation:

$$q_e = \frac{V_{sol.}(C_o - C_e)}{m} \quad \text{..... (1)}$$

$$\text{Removal\%} = \frac{(C_o - C_e)}{Co} * 100 \quad \text{..... (2)}$$

Where q_e is the quantity of adsorbed substance (mg/g), m is the adsorbent mass (g), C_o is the initial concentration (mg/L), C_e is the equilibrium concentration (mg/L) and V is the mixture volume (L). The influence of severalt factors such as the adsorbent loading, initial pH, temperature and ionic strength on adsorptive removal of RB dye were also studied.

3. Results and Discussion

3.1. Characterization of Carbon Nanospheres

3.1.1. FTIR analysis: The adsorption capacity of an adsorbent is affected by molecular structure and functional groups present on the surface. FTIR spectroscopy offers a fast and an efficient tool for identification of functional groups in synthesized materials. **Figure 2A** illustrates the FTIR spectra of carbon nanospheres and treated carbon nanospheres. The wide peak in both samples centered at 3433 cm^{-1} is assigned to the hydroxyl group (OH) stretching vibration of the carboxyl group or adsorbed water molecules. The peaks at 2927 and 2861 cm^{-1} are assigned as CH_2 and CH_3 stretching vibration, respectively. A weak peak observed at 1630 cm^{-1} is for C=C of graphitic carbon. The peak observed at 1052 cm^{-1} is because of C-O stretching frequency (2).

3.1.2. X-ray analysis: X-ray diffraction technique was used to identify the crystal structure of the fabricated carbonaceous materials. **Figure 2B** shows the X-ray diffraction spectra of carbon nanospheres PC and HC, it has been noticed the presence of a broad diffraction peak in 23.45^o due to the presence of the hexagonal graphite structure. While low intensity diffraction peak in 42.31^o are due to the presence of nanocarbons in the soot composition. The broad peaks in XRD spectra indicate the amorphous nature of carbon nanospheres. The X-ray diffraction spectra of carbon nanospheres with hydrogen peroxide (HC) appears peaks in (23.58^o, 41.39^o). The broader and less intensity diffraction peaks can be used as an evidence of small sized nanoparticles. The absence of other peaks in the spectra indicates that the prepared carbon nanospheres do not contain crystals and other elements (27, 28). The average particle size of synthesized carbon nanospheres can be calculated from the full-width at half-maximum of diffraction peaks (FWHM) using the Debye-Scherrer equation:

$$D = \frac{k\lambda}{\beta\cos\theta} \qquad \ldots\ldots\ldots\ldots\ldots\ldots (3)$$

Whereas **D** represent particle size, **k** is a dimensionless shape factor. The shape factor has a typical value of about 0.9, **λ** is the X-ray wavelength is value = 0.15056nm, **FWHM** (β) is the full width at half maximum of the peak, **θ** is the diffraction angle (deg.). The calculated average particle size distribution of carbon nanoparticles was around 43 nm for PC and 38 nm for HC.

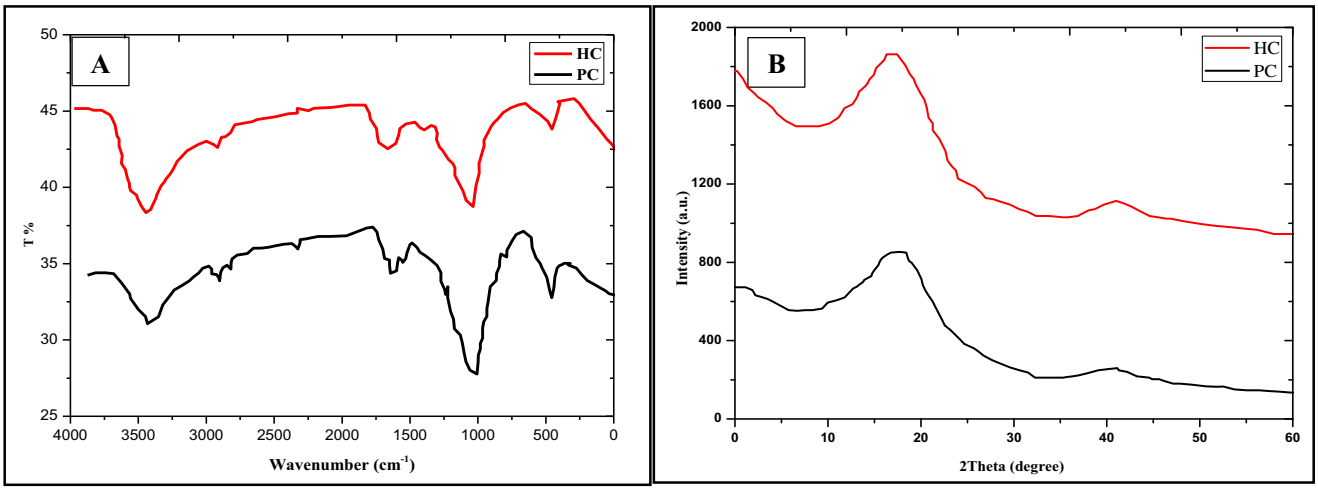

Fig. 2. A- FTIR spectra, B-XRD patterns of PC and HC

3-1-3. FE-SEM analysis: Scanning electron microscope was employed to investigate the surface morphology and characterization of synthesized materials. **Figure 3** shows that the synthesized carbon materials are of spherical shape, showing many aggregations due to the drying before FE-SEM analysis. The diameters of the PC and HC are in the range of (51-91) nm and (43-106) nm, respectively. The SEM micrographs showed the roughness of the surface of carbon nanospheres, whereas many large pores and cavities with irregular particles and channel arrays were clearly found on the surfaces of the two carbon materials. This shows the presence of porous structure which is responsible for the appropriate surface area of both synthesized materials. The synthesized materials were determined to have an appropriate surface characteristic for the adsorption processes of pollutants (29).

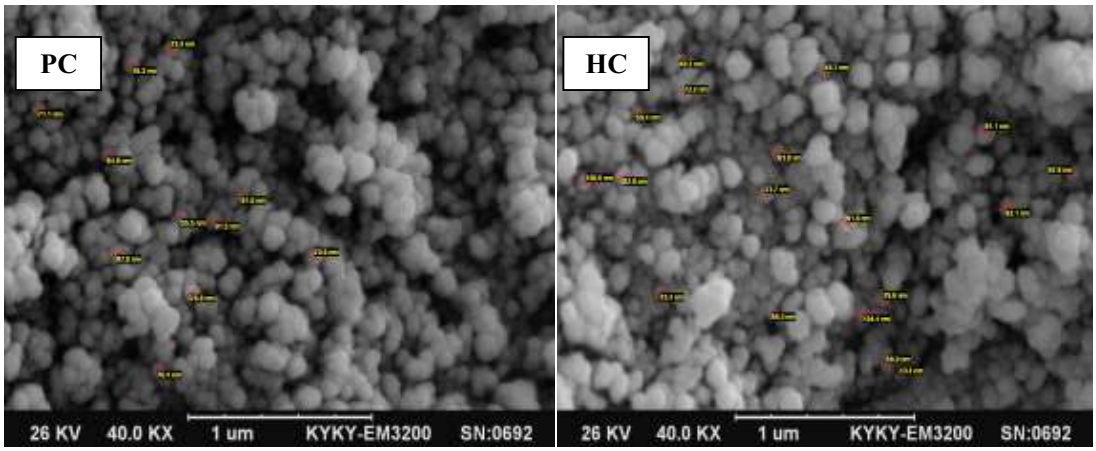

Fig. 3. FE-SEM photographs of PC and HC

3-1-4. AFM analysis: AFM technique was used to determine the surface topography and the thickness of the prepared carbon nanospheres. The AFM analysis of carbon nanospheres (PC) illustrates that the thickness is 5 nm, which is attributed to the chemical nature and containing functional groups, while AFM analysis of treated carbon nanospheres (HC) shows that the thickness is 8 nm which is attributed to treating the carbon nanoparticle surface with hydrogen peroxide and this increases the thickness of the prepared material. **Table 1** shows the enhanced roughness of carbon nanosphere surface is supported by the observed negative values of skewness which mean the number of surface valleys is higher than the peaks. Also, kurtosis parameter is a statistical measure used to describe the flatness of the height distribution. While, R_{ku} <3 for both carbon nanospheres samples could by described as spiky surfaces(30).

Table 1: The topographic parameterss of ynthesized carbon nanospheres

Amplitude Factors	PC	HC
R_a (nm)	0.681	1.26
R_q	0.796	1.53
R_{sk}	-0.262	-0.289
R_{ku}	1.95	2.46
Thickness (nm)	5.00	8.00

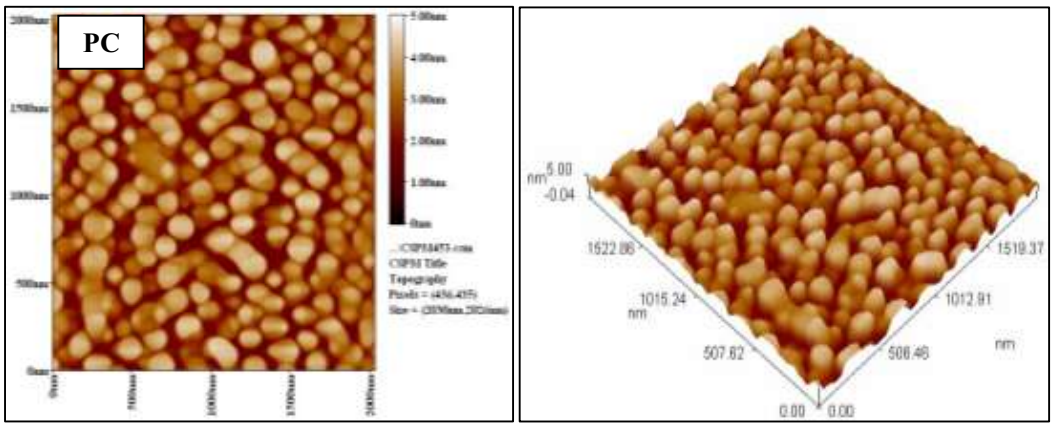

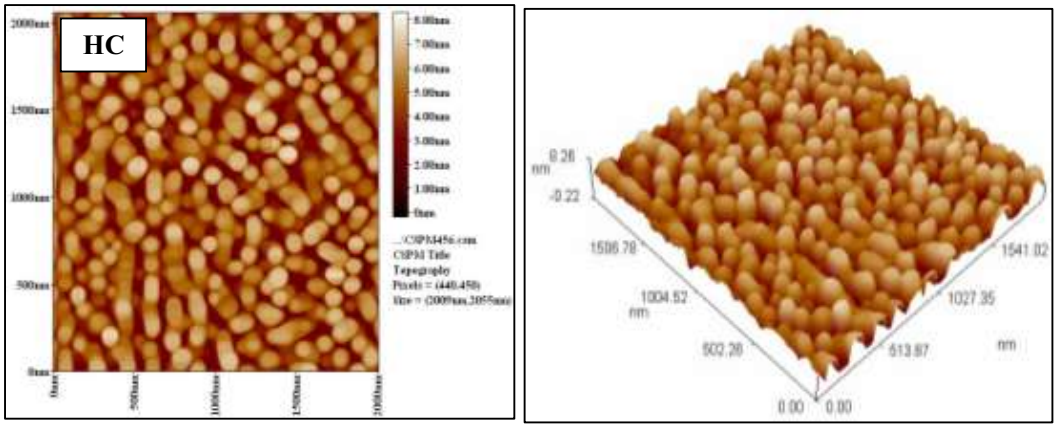

Fig. 4. AFM topographic images of PC and HC

3-1-5. TGA analysis: Thermogravimetric analysis providing information on the thermal stability of the synthesized samples. As shown in the **Figure 6A** TGA plot obtained indicates a gradual mass loss for both samples from 20-660 ^{o}C. Generally, the weight loss percentages of both samples are provided for two temperature ranges. The curve of carbon nanospheres (PC) displays two stages of quantity loss, the initial stage shows almost 5.206 % quantity loss in the range of 20-147.1 ^{o}C which in relation to the elimination of moisture from the sample. The second stage happened in the range of 147.1-643.23 ^{o}C with 80.37 % mass loss. An increasing loss of the materials in this temperature range could due to the decomposing of amorphous structure. For the modified sample with H_2O_2 (HC), it clearly found that the rate of mass loss is observed to be higher than PC sample. The mass loss was 5.744 % at temperatures range almost 20-171.8 °C, owing to the removal of adsorbed water molecules, hydroxyl and carboxyl functional groups. While mass loss about 89.35 % in the range 171.8-644.06 °C, due to pyrolysis of the graphitic structure (31). Although, the results show that the weight loss is slowed down above 600 ^{o}C, but the results indicate that the synthesized substances are of low thermal stability (8).

3-1-6. Raman analysis: Raman technology gives information about chemical composition, crystal nature and molecular interactions. Raman spectra show for the carbon nanospheres recorded in the 1000-2000 cm^{-1}. It was seen that there were two characteristic peaks around 1600 cm^{-1} and 1300 cm^{-1}. The first peak (D-band) refers to graphite structure and represents the order of the crystal lattice. The second peak (G-band) represents the disorder/defects of the crystal lattice. **Figure 5B** exhibits appearance of a broad **D** band at 1339.65 cm^{-1} and 1302.44 cm^{-1} for PC and HC, respectively, that is due to the amorphous nature of the graphite lattice. The G band reflects disordered carbon atoms and therefore highlights defects in the crystalline structure. Its intensity is inversely proportional to the crystal grain size. Furthermore, it is more intense than the G band indicating there to be a large amount of highly disordered graphite (32). The G band appears at 1590.01 cm^{-1} and 1571.34 cm^{-1} for PC and HC, respectively, which is attributed to the graphitic carbon, which is more ordered, symmetrical and crystalline. The intensity ratio of these two bands I_D/I_G = 0.94 and 0.98 for PC and HC, respectively this ratio indicates a high disorder percentage in the graphite structure (33).

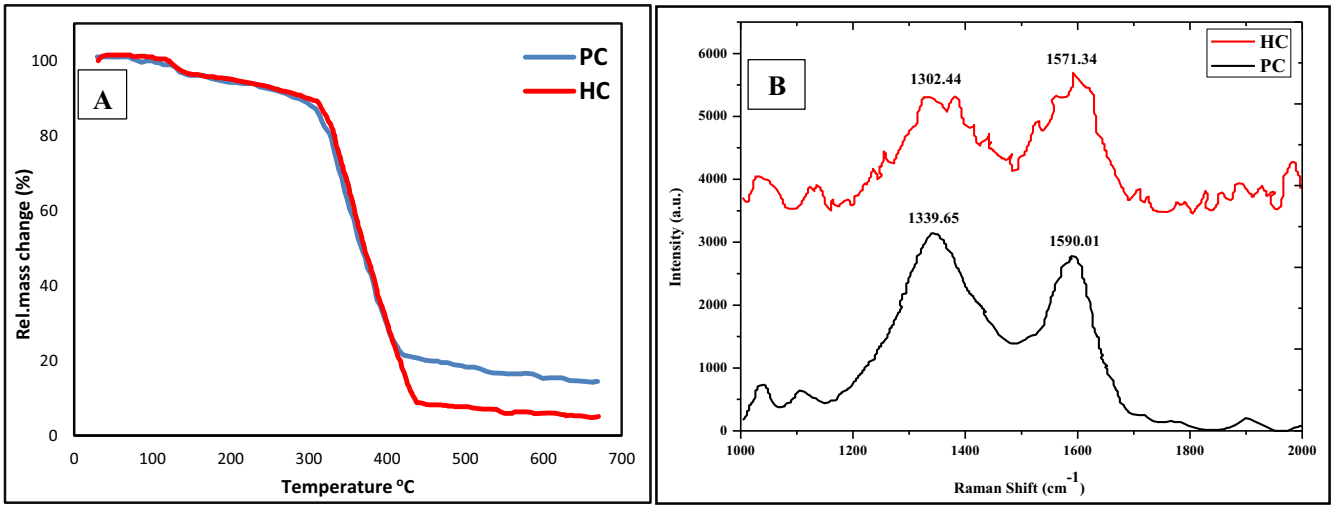

Fig. 5. A- TGA analysis, B- Raman spectrum of PC and HC

3-1-7. BET analysis: The Brunauer-Emmett-Teller (BET) technique is used to recognize the specific surface area by adsorption isotherms that are exhibited in **Figure 6**. The specific surface area and the pore diameter of carbon nanospheres (PC) was found to be 89.999 m^2/g and 39.079 nm, respectively. Where note of the value of the pore diameter indicates the mesoporous material. While treating carbon nanospheres appear is a high surface area up to 95.445 m^2/g and the pore diameter up to 40.166 nm. The results show the surface area of the treated carbon nanospheres is higher than of carbon nanospheres and therefore it is used as an adsorbent surface to remove dyes from aqueous solutions (34). The mean pore diameter indicates that both carbonaceous materials have mesoporous structures. As BET results revealed, both isotherms belong to typical IV adsorption behavior according to International Union of Pure and Applied Chemistry (IUPAC) (35). The characteristics features of IV isotherm is associated with monolayer adsorption followed by multilayer formation and capillary condensation. Controlling the texture parameters of surface of carbon nanospheres is important in adsorption and catalytic activities.

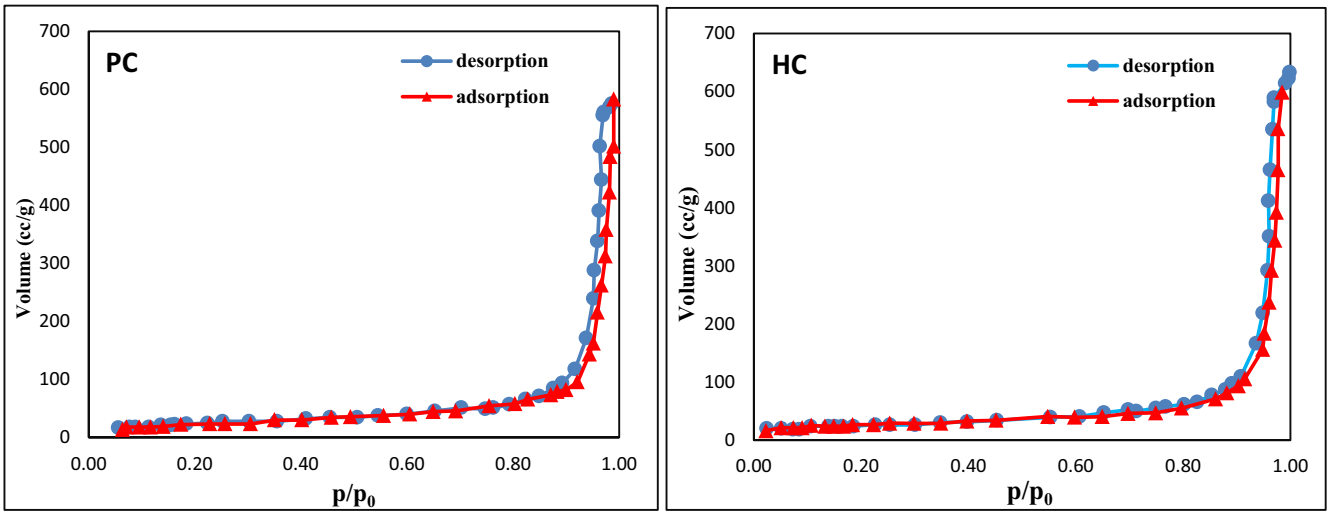

Fig. 6. N_2 adsorption and desorption curves of PC and HC

3-1-8. EDX analysis: EDX analysis is used to analyze the elemental composting of samples as shows in Table 2 and **Figure 7**. The spectrum of carbon nanospheres PC confirms the existence of carbon, oxygen and sulfur. The carbon nanospheres consist from 95.6 % carbon, 2.3% oxygen and 2.1 % sulfur. The sulfur element could be detected as residue from diesel. While the treated carbon nanospheres (HC) consist from 96.4 % carbon, 3.6% oxygen showing better purity. EDX of HC shows that no residuals were present on the carbon nanospheres treated with hydrogen peroxide. Modification of carbon nanoparticles surface with H_2O_2 assisted sonication at room temperature increased the surface oxygen functional groups.

Table 2: EDX data of PC and HC

Material	*C %*	*O %*	S	*C/O*
PC	95.6	2.3	2.1	41.56
HC	96.4	3.6	—	26.77

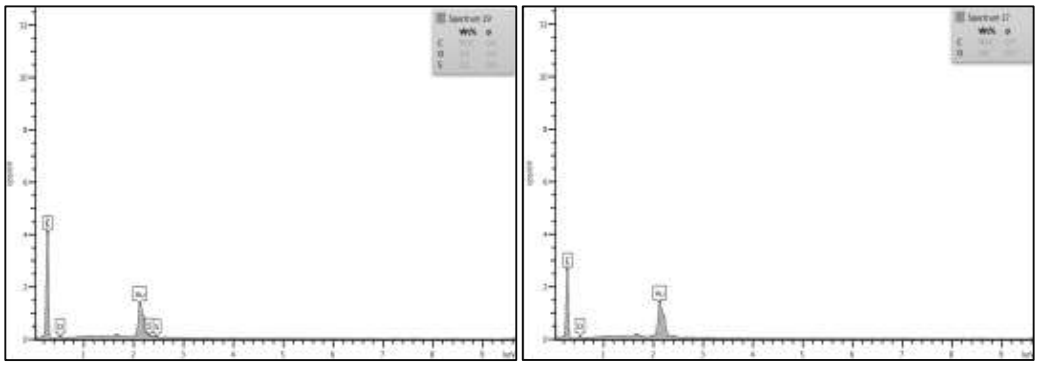

Fig. 7. EDX analysis of PC and HC

3-2. Adsorption Study

3-2-1. Effect of Adsorbents

Figure 8A shows the extent of adsorption of RB dye on both PC and HC adsorbents in aqueous solution. The results showed that HC demonstrates the highest RB adsorption capacity.

3-2-2. Effect of adsorbent HC dosage

The adsorption of the Rose Bengal dye on the surface of the carbon nanospheres has been studied in different weights in the range (0.001-0.01) g and shown in **Figure 8B**. The curve shows an increase in the adsorption ratio with increasing weight carbon nanospheres due to an increase in the surface area with an increase in the effective sites on the adsorbent surface (36).

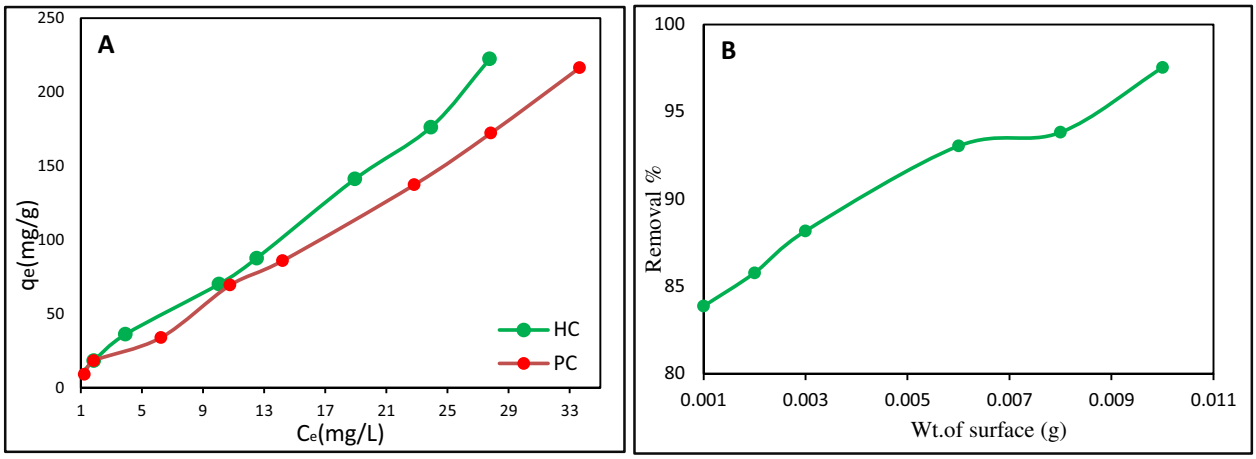

Fig. 8. A- Effect of Adsorbents and B- Effect of adsorbent doeage on the sorption capacity of Rose Bengal

3.2.3. Effect of Adsorption Time and Kinetics study

The effect of time on the adsorption of Rose Bengal dye over the carbon nanospheres surface has been studied using different times in the range (1-180) min. Where it was observed from **Figure 9A** that the amount of adsorbed material increases with the increase of time up to the saturation stage and then begins to decrease as a result of the separation of the dye from the adsorbent surface.

To understand the mechanism of dye adsorption on the carbon nanospheres surface, pseudo-first-order and pseudo-second-order equation models were studied. The equation below describes the pseudo-first-order model:

$$log(q_e - q_t) = log\ q_e - \frac{k_1}{2.303}\ t \quad \text{.....} \quad (4)$$

Whereas k_1 is the velocity constant first-order (1/min). Where to draw log (q_e − q_t) with time gives a straight line. The adsorbent quantity and speed constant first-order values can be found from the intercept and slope, respectively. The pseudo-second-order equation can be expressed as follows (37).

$$\frac{t}{q_t} = \frac{1}{k_2 {q_e}^2} + \left(\frac{1}{q_e}\right) t \quad \text{.....} \quad (5)$$

Whereas, the graph of the t/q_t values versus time display a linear relationship. The adsorbent quantity and speed constant second-order values can be found from the intercept and slope, respectively. (**Figure 9B**).

The kinetic factors for dye adsorption on the carbon nanospheres surface are shown in Table 3. Where note the high applicability of the adsorption process to pseudo-second-order model depending on the value of the correlation coefficient up to R^2 = 0.994. While the applicability to the pseudo-first-order model decreases due to the low value of the correlation coefficient up to R^2 = 0.946.

Table 3: kinetics factors of adsorption of Rose Bengal dye

Pseudo-first order	Pseudo-second order

	k_1	q_e	R^2	k_2	q_e	h	R^2
Rose Bengal	0.0069	30.985	0.946	0.00250	94.34	22.321	0.994

3.2.4. Effect of Temperature and Thermodynamic Study

To understand the effect of temperature on the adsorption process of the Rose Bengal dye, it was studied in 10, 20 and 30 ^{o}C. **Figure 9C** shows an increase in the amount of adsorbed material with increasing temperatures due to the increased speed diffusion dye on the most effective sites on the adsorbent surface, as well as the increase in kinetic energy leading to a strong attachment between the dye and the carbon nanospheres.

Thermodynamic functions are defined for the removing process of dye from the aqueous solutions and shown in Table 4. Where thermodynamic functions can be represented in the equations below:

$\Delta G = -RTlnK$ ..... (6)

$\Delta G = \Delta H - T\Delta S$ ..... (7)

$\Delta S = \frac{\Delta H - \Delta G}{T}$ ..... (8)

$lnK = \frac{\Delta S}{R} - \frac{\Delta H}{RT}$ ..... (9)

Where (ΔG°) is Gibbs free energy, (ΔH°) is ent6halpy change, (ΔS°) is change in entropy, T the absolute temperature (K) and (R) is general gas constant (8.314 J/mol K). ΔH° and ΔS° are calculated from the slope and intercept of van't Hoff plots of ln K versus T^{-1}. It observes from the values of thermodynamic functions that the positive value of the change in the enthalpy indicates that the adsorption process is endothermic. The negative value of the change in free energy indicates that the adsorption process is spontaneous and the positive value of the change in entropy indicates an increase in randomness between the adsorbate material and the adsorbent surface (38).

Table 4 :Thermodynamic parameters of adsorption of Rose Bengal dye

Dye	*Rose Bengal*
ΔH (kJ/mol)	95.611
ΔG (kJ/mol)	-168.07
ΔS (J/mol/K)	52.80
Equilibrium constant (K)	1.509

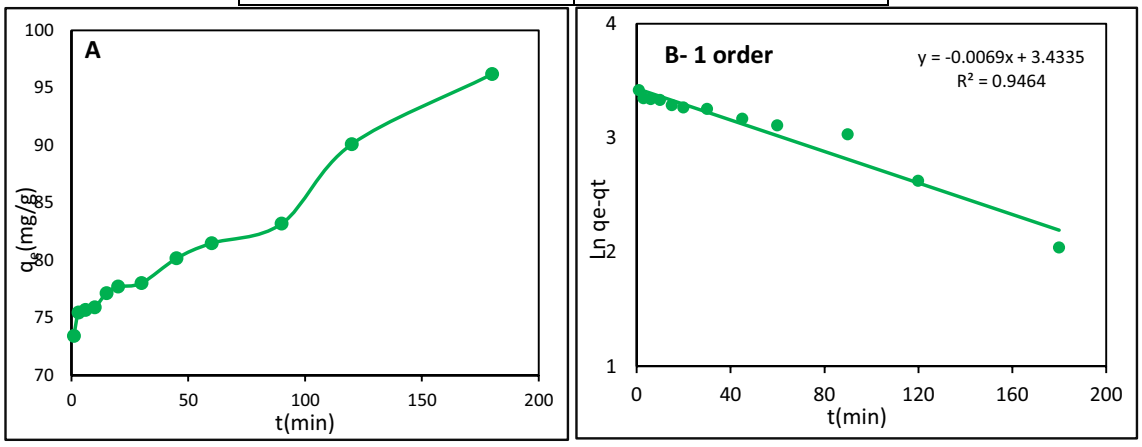

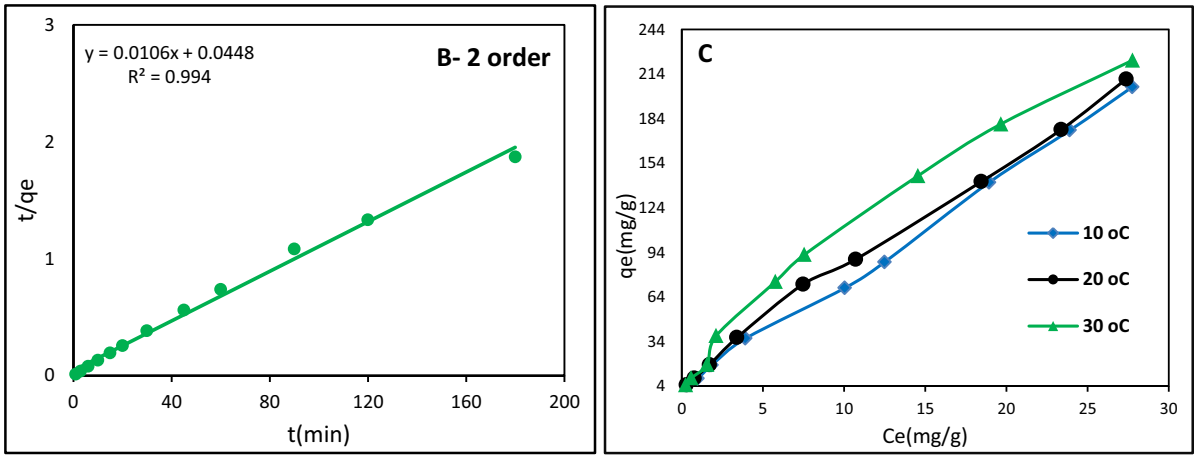

Fig. 9: A- Effect of Adsorption Time, B-Pseudo-first order and Pseudo-second order kinetics and C- Effect of temperature on the adsorption capacity of Rose Bengal dye

3.2.5. Adsorption Isotherm studies

Adsorption isotherm is the relationship between the amount of adsorbate and the residual concentration in the solution. The adsorption equilibrium data were tested using Langmuir, Freundlich and Tempkin isotherms. The equations below show the Langmuir, Freundlich, and Temkin models:

$$\frac{C_e}{q_e} = \frac{C_e}{q_m} + \frac{1}{K_L\, q_m} \quad \text{..... (10)}$$

$$log\, q_e = log\, K_f + \frac{1}{n} log C_e \quad \text{..... (11)}$$

$$q_e = BlnK_T + BlnC_e \quad \text{..... (12)}$$

Whereas (K_L, K_F, K_T) are the adsorption constants for all models, q_m is the maximum adsorption quantity (mg. g^{-1}) and n is the linear factor. Langmuir isotherm assumes monolayer adsorption of adsorbed molecules on homogeneous sites of the adsorbent surface. Freundlich isotherm assumes multilayer adsorption of adsorbed molecules on heterogeneous sites of the adsorbent surface. Lastly, the Temkin isotherm assumes adsorption as the interactions between adsorbate and adsorbent species (39).

It observed from **Figure 10** that adsorption of Rose Bengal dye on the surface of carbon nanospheres does not fitting to the Langmuir and Temkin isotherms depending on the values of the correction coefficients. While it fitting to Freundlich isotherm, this indicates that the adsorption process is multilayer.

Table 5: Langmuir, Freundlich and Tempkin isotherm constants

	Langmuir			Freundlich			Tempkin		
	K_L	q_m	R^2	K_F	n	R^2	K_T	B	R^2
Rose Bengal	0.032	225. 61	0.818	12.66	1.200	0.997	108.16	0.022	0.828

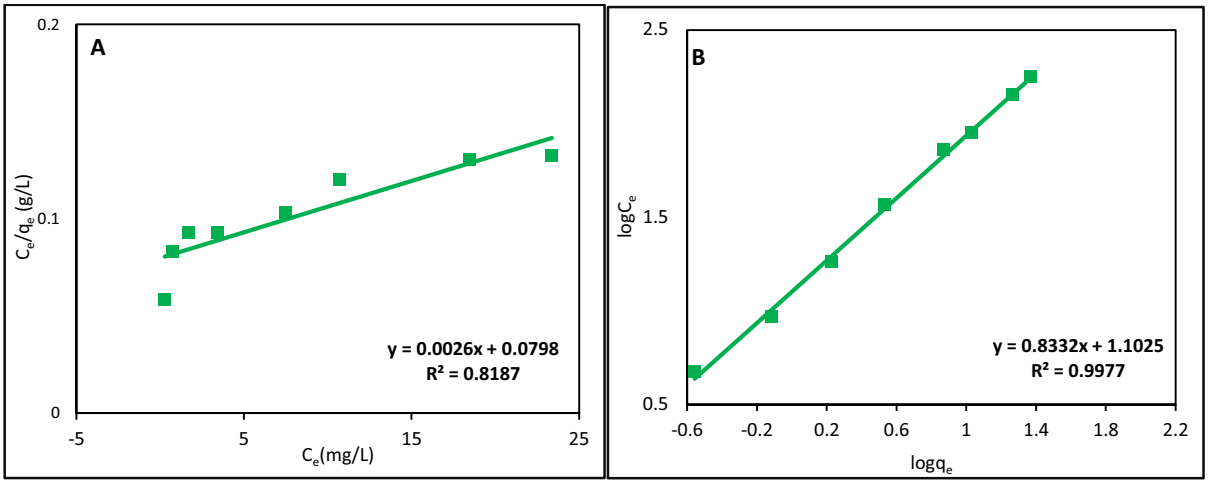

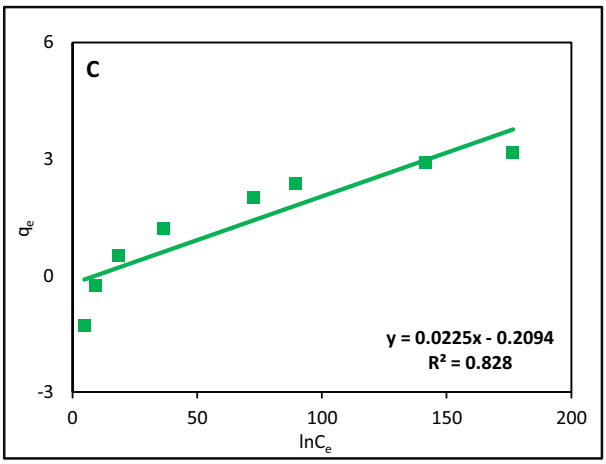

Fig. 10. Adsorption isotherms A- Langmuir, B- Freundlich, C- Tempkin.

3.2.6. Effect of initial pH

The acidic function of the dye solution is one of the most important factor affecting the adsorption process as a result of an increase or decrease in positive and negative charges. Where the acid function was studied in the range (1.0-12.0) and shown in **Figure 11A**. The results show a decrease in the adsorption capacity with an increase in the acidic function due to the increase in positive charges in the acidic medium and consequently the effective sites on the adsorbent surface increase with increasing electrostatic attraction between the dye (negative charges) and the adsorbent surface (positive charges). In contrast, the decrease in the adsorption capacity in the basic medium due to the competition between the negative charges of

the base and the negative charges of the dye on the active sites of the adsorbed surface.

3.2.7. Effect of salt

The effect of salts is one of the factors affecting the dye removal process from aqueous solutions. Where the ionic intensity was studied using different weights (0-0.4 gm) of sodium chloride salt. It observed from **Figure 11B** that the percentage of dye removal decreases with the increasing weight of sodium chloride (NaCl) salt due to the ability of the salt to block the connection between the dye (negative charges) and the carbon nanospheres (positive charges).

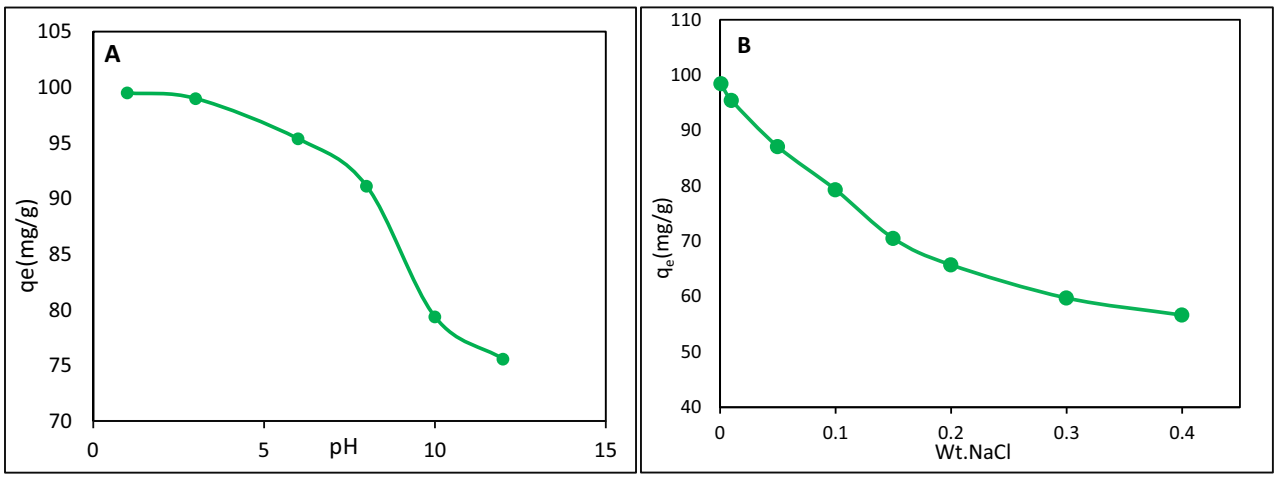

Fig. 11. A- B-Effect of pH solution and Effect of ionic strength on adsorption process

5. Literature Survey

These results confirm that carbon nanospheres were successfully synthesized from oil diesel, with promising surface properties when, compared to other adsorbents fabricated from other sources using thermal fabrication methods. E.g. activated carbon obtained from Terminalia catappa Linn fruit shells (40) and dried leaves of Aloe barbadensis (41) which degraded 77.5% and 90.0%, respectively. Table 6 shows a comparison with other adsorbents adsorbents studies made for the adsorptive removal of different organic dyes.

Table 6: Application of some carbonaceous adsorbents for the removal of some dyes from aqueous solutions.

Adsorbent	*Synthetic Method*	*Dye*	*R(%)*	*[Dye] mg/L*	*Contact time*	*Ref.*
CNs	Thermal	RB	97.5	50	180	This work
$ZnCl_2$-Activated carbon	Thermal	RB	77.5	50	160	(40)
Activated carbon	Thermal	RB	90.0	20	60	(41)
CNPs	Oxidation	MB	99.9	50	240	(42)

Magnetite/Carbon solution	Combustion	BR2	96.5	100	120	(43)
Coconut shell AC	Thermal	RB 19	82.1	50	50	(44)
Magnetic activated cNPs	Thermal	RR198	87.5	60	120	
Activated carbon	Thermal	MB	58.7	50	120	(45)
Activated carbon	Thermal	Rh.B	99.5	200	180	(46)
Activated carbon	Thermal	CR	99.2	50	240	(47)
Activated carbon	Thermal	MB	98	20	60	(48)
MFS	Grounding and Drying	RB	80	40	65	(49)

CNs: Carbon nanospheres; **RB**: Rose Bengal; **MB**: Methylene Blue; **RB2**: Basic Red 2; **RB19**: Reactive Blue 19; **Rh.B**: Rhodamone B; **RR198**: Reactive Red 198; **CR**: Congo Red; **MFS; Myristica fragrans Shells**

4. Conclusions

Carbon nanospheres were prepared by burning diesel. Analytical data show that the prepared material is nanoscale and has a particles size less than 50nm. Because the high surface area of the prepared material was used as an adsorbent surface to remove the Rose Bengal dye from the aqueous solutions. The adsorption kinetics showed that the reaction followed a false second-order model. Thermodynamic study showed that adsorption process occurs spontaneously and endothermically. As for adsorption isotherms models, does not fitting to the Langmuir and Temkin isotherms, while it applies to the Freundlich model and this indicates the adsorption reaction is monolayer. This study showed that the HC can be used as an efficient sorbent for RB dye removal in comparison with its non-treated sample (PC).

Acknowledgments

The authors are pleased to acknowledge the University of Al-Qadisiyah for providing the research facilities.

References

1. Li X, Rui M, Song J, Shen Z, Zeng H. Carbon and graphene quantum dots for optoelectronic and energy devices: a review[J]. Advanced Functional Materials. 2015, 25(31):4929-47.
2. Singh J, Nandi T, Ghosh S, Srivastava J, Tripathi S, Prasad N. Carbon nanoparticle synthesis, separation, characterization, and tribological property evaluation[J]. Separation Science and Technology. 2018, 53(14):2314-26.

3. Yallappa S, Manaf S, Shiddiky MJ, Kim JH, Hossain M, Shahriar A. Synthesis of carbon nanospheres through carbonization of areca nut[J]. Journal of Nanoscience and Nanotechnology. 2017, 17(4):2837-42.
4. Sun X, Sun H, Li H, Peng H. Developing polymer composite materials: carbon nanotubes or graphene[J]. Advanced Materials. 2013, 25(37):5153-76.
5. Yan Y, Miao J, Yang Z, Xiao F-X, Yang HB, Liu B, et al. Carbon nanotube catalysts: recent advances in synthesis, characterization and applications[J]. Chemical Society Reviews. 2015, 44(10):3295-346.
6. Rashid M, Ralph SF. Carbon nanotube membranes: synthesis, properties, and future filtration applications[J]. Nanomaterials. 2017, 7(5):99.
7. Kundu S, Chowdhury IH, Naskar MK. Hierarchical porous carbon nanospheres for efficient removal of toxic organic water contaminants of phenol and methylene blue[J]. Journal of Chemical & Engineering Data. 2018, 63(3):559-73.
8. Vivek D, Venkateswer M R, Prasad JS, Garima M, Kyong Y R, Hyeon J K and Dong H J, Carbon nanospheres synthesized via solution combustion method: their application as an anode material and catalyst for hydrogen production[J]. Carbon Letters. 2014, 15(3):198-202.
9. Huan W, Xiangui L, Zhiqiang M, Dan W, Linzhao W, Jieqiong Z, Lan S, and Feng Y, Hydrophilic mesoporous carbon nanospheres with high drug-loading efficiency for doxorubicin delivery and cancer therapy[J]. International Journal of Nanomedicine. 2016, 11:1793.
10. Kokorina AA, Prikhozhdenko ES, Sukhorukov GB, Sapelkin AV, Goryacheva IY. Luminescent carbon nanoparticles: synthesis, methods of investigation, applications[J]. Russian Chemical Reviews. 2017, 86(11):1157-71.
11. Hossain MA, Islam S, Synthesis of carbon nanoparticles from kerosene and their characterization by SEM/EDX, XRD and FTIR[J]. American Journal of Nanoscience and Nanotechnology, 2013, 1(2):52.
12. Liu J, Shao M, Chen X, Yu W, Liu X, Qian Y. Large-scale synthesis of carbon nanotubes by an ethanol thermal reduction process[J]. Journal of the American Chemical Society. 2003, 125(27):8088-9.
13. Benito P, Herrero M, Labajos F, Rives V, Royo C, Latorre N, and Monzon A, Production of carbon nanotubes from methane: use of Co-Zn-Al catalysts prepared by microwave-assisted synthesis[J]. Chemical Engineering Journal. 2009, 149(1-3):455-62.
14. Shao M, Li Q, Wu J, Xie B, Zhang S, Qian Y. Benzene-thermal route to carbon nanotubes at a moderate temperature[J]. Carbon. 2002, 40(15):2961-3.
15. Dikio ED. Morphological characterization of soot from the atmospheric combustion of kerosene[J]. Journal of Chemistry. 2011, 8(3):1068-73.
16. Dikio ED. Morphological characterization of soot from the atmospheric combustion of diesel fuel[J]. International Journal of Electrochemical Science, 2011, 6:2214-22.
17. Mohan AN, Manoj B. Synthesis and characterization of carbon nanospheres from hydrocarbon soot[J]. International Journal of Electrochemical Science, 2012, 7(10):9537-49.

18. Dikio D, Bixa N. Carbon nanotubes synthesis by catalytic decomposition of ethyne using Fe/Ni catalyst on aluminium oxide support[J]. International Journal of Applied Chemistry, 2011, 7:35-42.
19. Li C, Li M, Wang X, Feng W, Zhang Q, Wu B, Hu X. Novel Carbon Nanoparticles Derived from Biodiesel Soot as Lubricant Additives[J]. Nanomaterials. 2019, 9(8):1115.
20. Zhao X, Zhao T, Peng X, Hu J, Yang W. Catalyst effect on the preparation of single-walled carbon nanotubes by a modified arc discharge[J]. Fullerenes, Nanotubes and Carbon Nanostructures. 2019, 27(1):52-7.
21. Ganash EA, Al-Jabarti GA, Altuwirqi RM. The synthesis of carbon-based nanomaterials by pulsed laser ablation in water[J]. Materials Research Express. 2019, 7(1):015002.
22. Gutiérrez-G, Carmen J, Ambriz-T, Jael M, de Jesús C-N, José G-M, Francisco G, García-R, Diana L, García-G, Leandro Z-P, Luis O-V, Luis F, Richaud A and Méndez F. Synthesis of carbon spheres by atmospheric pressure chemical vapor deposition from a serial of aromatic hydrocarbon precursors[J]. Physica E: Low-dimensional Systems and Nanostructures. 2019, 112:78-85.
23. Yu K, Wang J, Song K, Wang X, Liang C, Dou Y. Hydrothermal Synthesis of Cellulose-Derived Carbon Nanospheres from Corn Straw as Anode Materials for Lithium ion Batteries[J]. Nanomaterials. 2019, 9(1):93.
24. Xu H, Yin X, Zhu M, Li M, Zhang H, Wei H, Zhang L and Cheng L. Constructing hollow graphene nano-spheres confined in porous amorphous carbon particles for achieving full X band microwave absorption[J]. Carbon. 2019, 142:346-53.
25. Zaib Q, Jouiad M, Ahmad F. Ultrasonic Synthesis of Carbon Nanotube-Titanium Dioxide Composites: Process Optimization via Response Surface Methodology[J]. ACS Omega. 2019, 4(1):535-45.
26. Dikio ED. Morphological characterization of soot from the atmospheric combustion of diesel fuel[J]. International Journal of Electrochemical Science. 2011, 6:2214-22.
27. Shooto ND, Dikio ED. Synthesis and characterization of diesel, kerosene and candle wax soot's[J]. International Journal of Electrochemical Science, 2012, 7:4335-44.
28. Lu P, Li C, Zeng G, Xie X, Cai Z, Zhou Y, Zhao Y, Zhan Q and Zeng Z. Research on soot of black smoke from ceramic furnace flue gas: Characterization of soot[J]. Journal of Hazardous Materials. 2012, 199:272-81.
29. Sarkar I, Raman R, Jayanth K, Jain A, Vora K. Characterization of Soot Microstructure for Diesel and Biodiesel Using Diesel Particulate Filter[J]. Innovative Design, Analysis and Development Practices in Aerospace and Automotive Engineering (I-DAD 2018): Springer, 2019. 153-61.
30. Alipour R, Hosseinnejad M, Elahi AS, Ghoranneviss M, RETRACTED: New perspective on morphological features of the zinc oxide thin films as a gas sensor[J]. Elsevier, 2016.

31. Hussain N B, Alshamsi HAH, Synthesis, morphological, structural and topological characteristics of carbon nanosphere derived from Iraqi diesel[J]. Journal of Physics: Conference Series; 2019: IOP Publishing.
32. Kaniyoor A, Ramaprabhu S A, Raman spectroscopic investigation of graphite oxide derived graphene[J]. Aip Advances. 2012, 2(3):032183.
33. Sadezky A, Muckenhuber H, Grothe H, Niessner R, Pöschl U, Raman microspectroscopy of soot and related carbonaceous materials: spectral analysis and structural information[J]. Carbon. 2005, 43(8):1731-42.
34. Popovicheva O, Persiantseva N, Tishkova V, Shonija N, Zubareva N, Quantification of water uptake by soot particles[J]. Environmental Research Letters. 2008, 3(2):025009.
35. Thommes M, Kaneko K, Neimark A V, Olivier J P, Rodriguez-R F, Rouquerol J and Sing K SW, Physisorption of gases, with special reference to the evaluation of surface area and pore size distribution (IUPAC Technical Report) [J]. Pure and Applied Chemistry. 2015, 87(9-10):1051-69.
36. Alwan SH, Alshamsi HA, Jasim LS, Rhodamine B removal on A-rGO/cobalt oxide nanoparticles composite by adsorption from contaminated water[J]. Journal of Molecular Structure. 2018, 1161:356-65.
37. Alwan S, Hussain N, Alshamsi H, Sahib I, Green Synthesis of S-and N-Codoped Carbon Nanospheres and Application as Adsorbent of Pb (II) from Aqueous Solution[J]. International Journal of Chemical Engineering. 2020, (2020):13.
38. Alwan SH, Alshamsi HA, Al-Hayder LS. Synthesis and characterization of rGO/Co_3O_4 composite as nanoadsorbent for Rhodamine 6G dye removal[J]. Desalianation and Water Treatment. 2018,114:320-31.
39. Gao Y, Li Y, Zhang L, Huang H, Hu J, Shah S M and Su X, Adsorption and removal of tetracycline antibiotics from aqueous solution by graphene oxide[J]. Journal of Colloid and Interface Science. 2012, 368(1):540-6.
40. Nandhakumar V, Rajathi A, Venkatachalam R, Ramesh K, Savithiri S. Adsorption of Rose Bengal dye from aqueous solution onto zinc chloride activated carbon[J]. SOJ Materials Science & Engineering, 2015, 3:1-9.
41. Arivoli S, Sundaravadivelu M, Elango K. Removal of basic and acidic dyes from aqueous solution by adsorption on a low cost activated carbon: Kinetic and thermodynamic study[J]. Indian Journal of Chemical Technology, 2008, (15):130-139.
42. Yang S-T, Luo J, Zhou Q, Wan J, Ma C, Liao R. Adsorption behaviour of methylene blue on carbon nanoparticles[J]. Micro & Nano Letters. 2012, 7(10):1060-3.
43. Muntean SG, Nistor MA, Muntean E, Todea A, Ianoş R, Păcurariu C. Removal of colored organic pollutants from wastewaters by magnetite/carbon nanocomposites: single and binary systems[J]. Journal of Chemistry. 2018, 2018.
44. Abdulraheem G, Bala S, Muhammad S, Abdullahi M. Kinetics, equilibrium and thermodynamics studies of CI Reactive Blue 19 dye adsorption on coconut shell based activated carbon[J]. International Biodeterioration & Biodegradation. 2015, 102:265-73.

45. Kuang Y, Zhang X, Zhou S. Adsorption of Methylene Blue in Water onto Activated Carbon by Surfactant Modification[J]. Water. 2020, 12(2):587.
46. Geçgel Ü, Üner O, Gökara G, Bayrak Y. Adsorption of cationic dyes on activated carbon obtained from waste Elaeagnus stone[J]. Adsorption Science & Technology. 2016, 34(9-10):512-25.
47. Lafi R, Montasser I, Hafiane A. Adsorption of Congo red dye from aqueous solutions by prepared activated carbon with oxygen-containing functional groups and its regeneration[J]. Adsorption Science & Technology. 2019, 37(1-2):160-81.
48. Luo L, Wu X, Li Z, Zhou Y, Chen T, Fan M and Zhao W. Synthesis of activated carbon from biowaste of fir bark for methylene blue removal[J]. Royal Society Open Science. 2019, 6(9):190523.
49. Waheeb AS, Alshamsi HAH, Al-Hussainawy MK, Saud HR. Myristica fragrans Shells as Potential Low Cost Bio-Adsorbent for the Efficient Removal of Rose Bengal from Aqueous Solution: Characteristic and Kinetic Study[J]. Indonesian Journal of Chemistry.